


Topological mechanism in the nonlinear power-law relaxation of cell cortex

Shao-Heng Li and Guang-Kui Xu ^{*}

Laboratory for Multiscale Mechanics and Medical Science, Department of Engineering Mechanics, State Key Laboratory for Strength and Vibration of Mechanical Structures, School of Aerospace Engineering, Xi'an Jiaotong University, Xi'an 710049, China

 (Received 27 May 2023; revised 4 September 2023; accepted 16 November 2023; published 18 December 2023)

Different types of cells exhibit a universal power-law rheology, but the mechanism underneath is still unclear. Based on the exponential distribution of actin filament length, we treat the cell cortex as a collection of chains of crosslinkers with exponentially distributed binding energy, and show that the power-law exponent of its stress relaxation should scale with the chain length. Through this model, we are able to explain how the exponent can be regulated by the crosslinker number and imposed strain during cortex relaxation. Network statistics show that the average length of filament-crosslinker chains decreases with the crosslinker number, which endows a denser network with lower exponent. Due to gradual molecular alignment with the stretch direction, the number of effectively stretched crosslinkers in the network is found to increase with the imposed strain. This effective growth in network density diminishes the exponent under large strain. By incorporating the inclined angle of crosslinkers into the model without in-series structure, we show that the exponent cannot be altered by crosslinker rotation directly, refining our previous conjectures. This work may help to understand cellular mechanics from the molecular perspective.

DOI: [10.1103/PhysRevE.108.064408](https://doi.org/10.1103/PhysRevE.108.064408)

I. INTRODUCTION

Many experiments showed that different types of cells exhibit a universal power-law rheology [1,2]. For instance, when subjected to constant stresses, cellular strain grows as a power law of time, $\varepsilon \propto t^\beta$ [3–6]; when subjected to constant strains, cellular stress decays as a power law of time, $\sigma \propto t^{-\beta}$ [7–10]; when subjected to oscillatory loads, the complex modulus varies as a power law of frequency, $G^* \propto \omega^\beta$ [11–16]. During these processes, the power-law exponent β can be delicately regulated, depending on the amplitude of applied strain/stress or the frequency of cyclical loads. Creep experiments showed that β remains unchanged when the stress is increased slightly [5,6], but starts to grow if the stress is increased by orders of magnitude [3]. Relaxation experiments revealed that β appears to be stable under large strains [7], while small-strain experimental measurements are lacking. Oscillatory experiments on *in vitro* actin networks demonstrated that β decreases with the loads [17–19]. Furthermore, molecular simulations suggested power-law relaxation of cortical networks as well [20,21], with the scaling exponent β increasing with the decline of imposed strain [20], like inert soft glassy matter [22]. Molecular simulations also showed that the mean-squared displacement of motors on actin networks grows anomalously as a power law of time [23]. These ubiquitous and robust power-law features are independent of cell types, cell states, or experiment methods, implying general biomechanical principles underneath.

Although many theoretical efforts have been devoted to understanding the cellular rheology, the underlying mesoscopic

mechanisms remain ambiguous. The remarkable soft glassy rheology (SGR) model can capture the stress-induced β growth in creep responses, but could not explain its variation with respect to strain in relaxation [24–26]. A recent mesoscopic network dynamics model investigated the change of β with respect to external strain or crosslinker number in cortex relaxation using molecular simulations, but the interpretation was merely qualitative [20]. Macroscopic self-similar hierarchical models, on the other hand, studied how β varies with cellular stiffness, mainly focusing on the effect of cell architecture embodied in different cellular hierarchies [27,28]. Currently, a physical understanding on the influence of external loads on β is still lacking.

II. MODEL

Here we present a minimal model to illuminate how the power-law exponent β can be regulated through a topological mechanism during cell cortex relaxation (Fig. 1). The cortex network is considered as a collection of crosslinker chains, each composed of d harmonic springs connected in series, with spring constant k and rest length l_0 . When subjected to a global strain ε , crosslinkers dissociate with a rate of thermal activation form, written as

$$\Gamma(E, \varepsilon) = \gamma \exp \left[- \left(E - \frac{kl_0^2 \varepsilon^2}{2} \right) / \xi \right], \quad (1)$$

where γ represents the rate constant, E the binding energy, and ξ the thermal energy coupled with bond rupture. Following the paradigm of the SGR model, we consider the crosslinker dissociation as a thermal-activated hop out of a harmonic well. This equation differs from the well-known Bell's equation only in the well shape [29], and the physical

^{*}Corresponding author: guanguixu@mail.xjtu.edu.cn

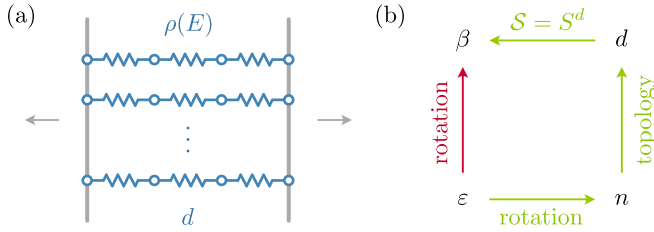


FIG. 1. Topological mechanism of cortex relaxation. (a) A minimal model of a cell cortex, which is abstracted as many molecular chains in parallel, each composed of d crosslinkers. The binding energy of crosslinkers is exponentially distributed, described by the probability density $\rho(E)$. (b) A downstream “signaling cascade” of the external strain ε , crosslinker number n , chain length d , and ultimately the power-law exponent β in cell cortex relaxation (green pathways: $d \rightarrow \beta$, $n \rightarrow d$, and $\varepsilon \rightarrow n$). Direct regulation by external strain through rotation is forbidden (red pathway: $\varepsilon \rightarrow \beta$).

nature behind both is the thermal activation over an energy barrier. Such a difference does not affect our following derivation, since Eq. (4) below holds irrespective of the form of τ_m .

In the real cortex, since actin filaments are semiflexible and of exponentially distributed length [30,31] and shorter filaments could exert larger forces due to their higher stiffness, crosslinkers bound to filaments of smaller length will dissociate with larger rate even under the same global strain. Such an acceleration effect of random length of filaments turns out to be equivalent to that of the similarly distributed binding energy of crosslinkers (see Appendix A). Hence the binding energy E in the dissociation rate is assumed to be exponentially distributed as well, with a probability density $\rho(E) \propto \exp(-E/\eta)$, where η is the mean value of binding energy E . In this manner, the disordered nature of the cell cortex is essentially subsumed into the randomness of binding energies, and the deformation of filaments is not considered explicitly. Once a crosslinker dissociates, the stress stored in the entire molecular chain is released immediately, and the crosslinker rebinds with a new binding energy according to the probability density function $\rho(E)$. The aim of this model is to explain the power-law relaxation of the cell cortex through the dissociation dynamics of crosslinkers and topological structure of the network, as suggested by previous experiments [15] and simulations [20,21], whereas effects such as polymerization and depolymerization of filaments, viscous flow of filaments within the cytoplasm, steric interaction between filaments, or myosin contractility will be investigated in the future.

In the initial steady state (i.e., $\varepsilon = 0$), the unbinding and rebinding of crosslinkers reach thermodynamic equilibrium, and thus the fraction $P(E)$ of crosslinkers with a specific binding energy E should satisfy

$$P(E)\Gamma(E, 0) = \rho(E) \int_0^\infty P(E)\Gamma(E, 0)dE, \quad (2)$$

in which the left-hand side reflects the number of crosslinkers that dissociate with this binding energy E and then rebind with possible binding energies, while the right-hand side reflects the number of crosslinkers that dissociate with any binding energies and then rebind with the binding energy E . This

equation basically states that the overall rate at which the system loses (through unbinding) and regains (through rebinding) a given binding energy E must be equal. The solution to Eq. (2) is

$$P(E) \propto \exp(-E/\eta) \exp(E/\xi), \quad (3)$$

which describes the initial state of the model. Here we assign $k = 16$ pN/nm and $l_0 = 50$ nm [32], along with $\gamma = 0.15$ s $^{-1}$ and $\xi = 1.2\eta = 250k_B T$ (see Appendix B) to ensure that the initial distribution $P(E)$ is normalizable and that the crosslinker strength for typical binding energy η conforms to experimental results [33]. The global stress σ at any time t is calculated by the sum of stresses over all chains.

The stochastic dissociation of crosslinkers can be simulated through the standard Gillespie algorithm [34,35]. Upon strain application, the lifetime of each crosslinker is tentatively calculated as $\Gamma^{-1}(E, \varepsilon) \ln(1/u)$, with u being a random number uniformly distributed on the interval $[0, 1]$ and regenerated each time. Then, the lifetime of each crosslinker chain is calculated as the minimum lifetime amongst its d components. The stress stored in each chain is released when its lifetime is reached. Recording the stress at the time of each chain rupture event, one obtains the history of stress relaxation. Using this model, we can investigate how β can be regulated by upstream parameters, such as the chain length d , and further the crosslinker number n and global strain ε in the network [Fig. 1(b)], discussed in detail as follows.

III. RESULTS AND DISCUSSION

A. The pathway of $d \rightarrow \beta$

Under a global strain $\varepsilon = 5\%$, we plot the stress relaxation curves on a log-log scale for $d = \{1, 2, 3\}$ in Fig. 2(a). The range of $d \in \mathbb{N}$ is chosen to match network statistics (Fig. 3). The curves here are the results of individual simulations, whose fluctuation is negligible due to the large number of crosslinkers $n \sim 10^4$. On each curve, the number of data points is n/d , since the stress is released only when a chain is ruptured. It can be seen that the stress decays with time in a power-law form, $\sigma \propto t^{-\beta}$, for sufficiently large time $t \gg \gamma^{-1}$, and the power-law exponent β increases with the chain length in proportion, as shown in Fig. 2(b).

This can be understood by analyzing the mean lifetime of crosslinker chains. For $d = 1$, each chain is composed of only one crosslinker, whose mean lifetime is the inverse of its dissociation rate and can be expressed as $\tau = \tau_m e^{E/\xi}$, with $\tau_m = \gamma^{-1} \exp(-kl_0^2 \varepsilon^2 / 2\xi)$ being the minimum mean lifetime. As a function of the binding energy E , the complementary cumulative distribution function of τ can be derived from the initial distribution $P(E)$ as

$$\begin{aligned} S(\tau') &= \Pr(\tau > \tau') \\ &= \int_{\xi \ln(\tau'/\tau_m)}^\infty P(E)dE \\ &\propto \tau'^{1-\xi/\eta}, \end{aligned} \quad (4)$$

where the prime denotes a given value of τ to discriminate it from the random variable. This function gives the probability that a crosslinker can survive beyond τ' , or in other words,

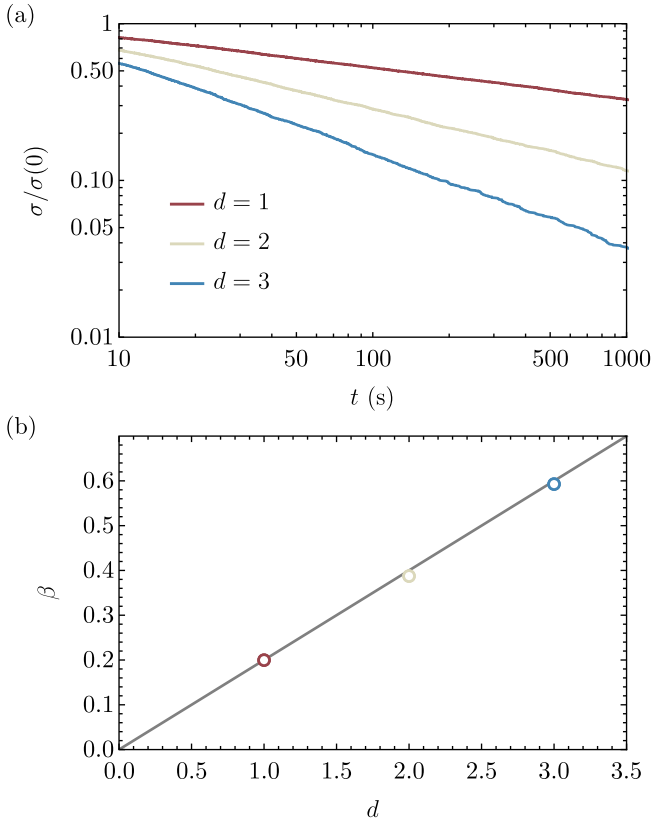


FIG. 2. Power-law relaxation of the minimal model. (a) Under different chain lengths $d = \{1, 2, 3\}$, the stress decays as a power law of time, $\sigma \propto t^{-\beta}$. (b) The exponent β is proportional to the chain length d , which can be fitted by a linear curve, $\beta(d) = d\beta(1)$. The number of crosslinkers is 10^4 .

the fraction of crosslinkers that remain bound at a given time. Since each crosslinker bears equal force, the normalized mean global stress at time t is thus $\sigma(t)/\sigma(0) = S(t) \propto t^{1-\xi/\eta}$, and accordingly $\beta(1) = \xi/\eta - 1 = 0.2$.

When each chain is composed of multiple crosslinkers ($d > 1$), its mean lifetime is determined by the most short-lived component, and hence can be expressed as $\bar{\tau} = \min(\tau_1, \dots, \tau_d)$, where $\{\tau_i\}_{i=1}^d$ is the mean lifetime of each component crosslinker. The complementary cumulative distribution function of $\bar{\tau}$ can be derived from the above single-molecule result. Noticing that $\bar{\tau} > \bar{\tau}'$ if and only if $\tau_i > \bar{\tau}'$ for any $1 \leq i \leq d$, and that each τ_i is independent, we have

$$\begin{aligned} S(\bar{\tau}') &= \Pr(\bar{\tau} > \bar{\tau}') \\ &= \prod_i^d \Pr(\tau_i > \bar{\tau}') \\ &= S^d(\bar{\tau}'), \end{aligned} \quad (5)$$

where the prime denotes a given value of $\bar{\tau}$ to discriminate it from the random variable. The above equation gives the probability that a chain can survive beyond $\bar{\tau}'$, or in other words, the fraction of chains that remain intact at a given time. Since each chain bears equal force, the normalized mean

global stress at time t is thus $\sigma(t)/\sigma(0) = S(t) \propto t^{(1-\xi/\eta)d}$, and accordingly $\beta(d) = (\xi/\eta - 1)d = d\beta(1)$, accounting for the results in Fig. 2.

B. The pathway of $n \rightarrow d$

In microrheological experiments on cells, the power-law exponent has been shown to decrease with the overexpression of intermediate filaments during relaxation [9], and increase with the reduction of cytoskeleton polymerization or crosslinker concentration during creep responses [6,36], suggesting cells tend to be more fluidlike when the spatial density of the cytoskeletal network descends. This can be understood through statistics on filament-crosslinker chain length under different crosslinker density in the cell cortex, whose configuration can be generated within a three-dimensional periodic box, with filaments considered as rigid rods and crosslinkers as Hookean springs (see Appendix C).

We generate cortex networks for a series of crosslinker numbers $n = \{4, 5, 6, 7, 8, 9, 10\} \times 10^3$. The length of filament-crosslinker chains can be characterized by the concept of graph distance in graph theory [37], which is defined as the minimum number of crosslinkers d_{ij} required to connect a pair of filaments $\{i, j\}$. When averaged over all filament pairs, the quantity $\langle d_{ij} \rangle$ characterizes the mean length of force-bearing chains in the network. This parameter may be regarded as an analog of d in the minimal model (see Appendix D), although it cannot reach the value 1 that demands any two filaments be connected in the network. The relationship between $\langle d_{ij} \rangle$ and n is plotted in Fig. 3, indicating that the molecular chains become longer as the network becomes sparser. This is essentially the same as that in Ref. [20], but obtained from new networks here. Since a larger chain length gives rise to a higher power-law exponent [see Fig. 2(b)], β should decrease with the growth of crosslinker number n , as reported in previous experiments [6,9,36] and simulations [20].

C. The pathway of $\epsilon \rightarrow n$

Our previous simulations on a cortex network show that the power-law exponent of relaxation may decrease with the

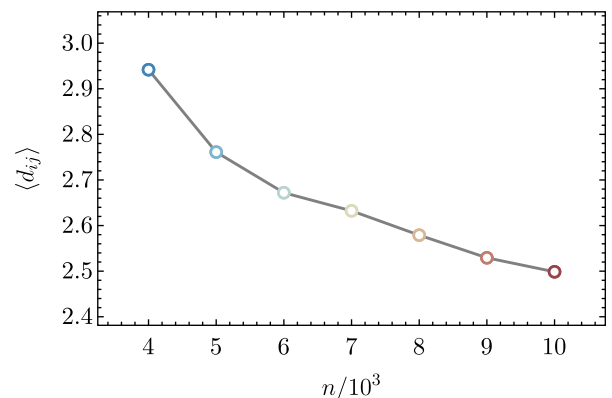


FIG. 3. Relationship between the average length of filament-crosslinker chains $\langle d_{ij} \rangle$ and the total number of crosslinkers n .

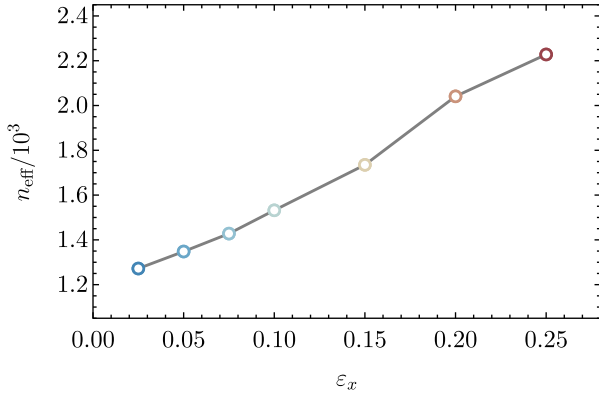


FIG. 4. Relationship between the number of effective crosslinkers n_{eff} and the external strain ϵ_x imposed on a network with $n = 5000$ crosslinkers.

imposed uniaxial strain [20], suggesting the cortex network behaves like inert soft glassy matters [22]. This can be understood through the strain-dependent variation of an “effective” crosslinker number n_{eff} , essentially defined as the number of crosslinkers whose deformation exceeds the strain imposed on the cortex.

We generate a cortex network with $n = 5000$ crosslinkers and stretch it with a series of uniaxial strains $\epsilon_x = \{2.5, 5, 7.5, 10, 15, 20, 25\} \times 10^{-2}$. The equilibrium network configurations can be obtained through the standard Metropolis algorithm [20,38]. Since the crosslinkers are constantly bombarded by the thermal bath, the part of molecular extension that is actually induced by external mechanical load, i.e., mechanical deformation, should be estimated as the apparent deformation directly extracted from the simulation minus the scale of thermal fluctuation. Hence, we write the mechanical deformation as $\Delta_{\text{mech}} = \Delta - \Delta_{\text{ther}}$, where $\Delta_{\text{ther}} = \sqrt{k_B T/k}$ is the standard deviation in thermal vibration of a harmonic spring, a consequence of Boltzmann distribution [39]. To measure how many crosslinkers are actually stretched by the imposed strain, we define the effective crosslinker number n_{eff} as the number of crosslinkers whose mechanical strain exceeds the threshold ϵ_x , or in terms of apparent deformation, $\Delta > l_0 \epsilon_x + \Delta_{\text{ther}}$. The relationship between n_{eff} and ϵ_x is plotted in Fig. 4, in which the number of effective crosslinkers robustly grows with the uniaxial strain. This is because crosslinkers tend to align with the stretch direction as the strain increases [20]. Therefore, effectively, the number of molecules is increased by the strain. Since larger molecular density leads to smaller chain length (see Fig. 3), which would further diminish the exponent, β should decrease with the external uniaxial strain, explaining the results in previous simulations [20] and experiments performed on inert soft glassy colloids [22].

D. The pathway of $\epsilon \rightarrow \beta$

An intuitive hypothesis is that the rotation of crosslinkers could decrease the power-law exponent directly, as their alignment with the stretch direction seems to solidify the network [20]. However, such an understanding is quite obscure. In fact,

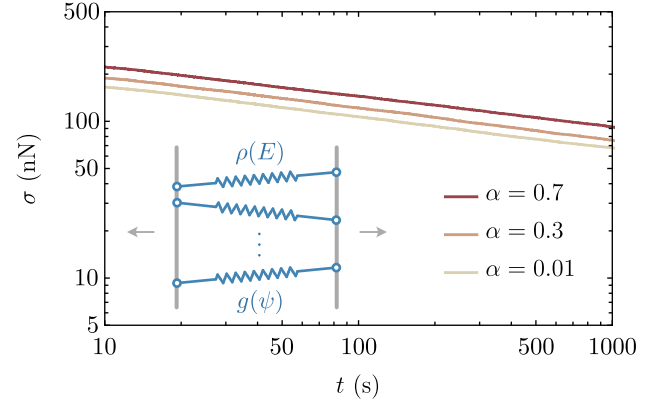


FIG. 5. Relaxation of minimal model with molecular rotation but without topological structure. The power-law exponent remains unchanged irrespective of the angle distribution. Inset: Minimal model where crosslinkers are endowed with random inclined angle ψ with respect to the horizontal direction, while their in-series connection is removed. The number of crosslinkers is 10^4 in the minimal model.

here we show that without the in-series structure of molecular chains, the exponent would always be $\beta \equiv \beta(1)$, no matter what form the strain energy distribution takes (Fig. 5).

In this scenario, the system in Fig. 1(a) becomes a collection of crosslinkers with random binding energy E and random inclined angle ψ with respect to the horizontal direction. Hence, the crosslinker extension is no longer $l_0 \epsilon$, but depends on its orientation, and can be approximated by $l_0 \epsilon \cos^2 \psi$ under small strains. By replacing the strain energy term in the original dissociation rate correspondingly, one obtains the new dissociation rate $\Gamma(E, \epsilon, \psi)$. Once the distribution of ψ is specified, the stochastic dissociation of crosslinkers can be simulated through the aforementioned standard Gillespie algorithm. Based on simulation data [20], we fit the probability density of $\psi \in (0, \pi/2)$ as a linear function, $g(\psi) = (\pi/4 - \psi)\alpha + 2/\pi$, where $\alpha = 0$ corresponds to the uniform distribution of orientations and $0 < \alpha < 8/\pi^2$ corresponds to the uneven distribution of orientations. Under a uniaxial strain $\epsilon = 5\%$, we plot the relaxation curves on a log-log scale for $\alpha = \{0.01, 0.3, 0.7\}$ in Fig. 5, where the exponent remains $\beta = 0.2$ even for the smallest α that corresponds to the most scattered distribution.

This can be understood through the lifetime distribution of inclined crosslinkers. Note that the orientation distribution of crosslinkers affects their lifetime through the *strain energy term* in its dissociation rate. Denote the strain energy of crosslinkers as $\Psi \in (0, \infty)$ with a probability density $h(\Psi)$. The mean lifetime can be expressed as $\hat{\tau} = \gamma^{-1} e^{(E-\Psi)/\xi}$, where the distribution of binding energy $E \in (0, \infty)$ is described by $P(E)$ for crosslinkers in the initial steady state. Since E and Ψ are independent, the complementary cumulative distribution function of $\hat{\tau}$ can be derived from $P(E)$ and $h(\Psi)$ as

$$\begin{aligned} \mathfrak{S}(\hat{\tau}') &= \Pr(\hat{\tau} > \hat{\tau}') \\ &= \iint_{E-\Psi > \xi \ln(\hat{\tau}'\gamma)} P(E)h(\Psi)dE d\Psi \\ &\propto \hat{\tau}'^{-\beta(1)} \end{aligned} \quad (6)$$

where $\hat{\tau}' > \gamma^{-1}$ and the prime denotes a given value of $\hat{\tau}$ to discriminate it from the random variable. The above relation is irrespective of the functional form of $h(\Psi)$. Assuming each crosslinker roughly bears equal force and using the same argument for stress relaxation as in the case of $d = 1$, one can obtain the normalized mean global stress at time $t > \gamma^{-1}$ as $\sigma(t)/\sigma(0) = \mathfrak{S}(t) \propto t^{-\beta(1)}$. For the less concerned $\hat{\tau} < \gamma^{-1}$ regime, if we arbitrarily choose $h(\Psi) \propto \exp(-\Psi/\zeta)$, the complementary cumulative distribution function will be $\mathfrak{S}(\hat{\tau}) = 1 - (\hat{\tau}\gamma)^{\xi/\zeta} \frac{\beta(1)}{\beta(1)+\xi/\zeta}$, which describes the transition of the relaxation curve from initial constant value to a power-law form. Therefore, its slope in a log-log plot is always below $\beta(1)$ for $\zeta \in (0, \infty)$. Neither of these two regimes can explain the exponent growth under small strains [20,22]. Since geometric factors such as orientation or stress distribution of crosslinkers affect the dissociation dynamics through the strain energy Ψ eventually, they can only alter the prefactor of the power law (the intercept of the relaxation curve), but not its exponent (the slope of the relaxation curve), in the absence of network topological structure.

IV. CONCLUSIONS

In summary, we present a ‘‘signaling cascade’’ that summarizes how the exponent β can be regulated by the molecular chain length d , how d can be regulated by the crosslinker number n , and how n can be regulated by the external strain ε in a downstream manner during the nonlinear power-law relaxation of the cell cortex, as shown in Fig. 1(b). Through a minimal model, we demonstrate how the exponent can be affected by the chain length. Since the stress of the entire chain is released once a crosslinker ruptures, the longer the chain, the faster the relaxation, whereby the exponent is raised. In real cortical networks, network statistics show that the average length of filament-crosslinker chains decreases as the network gets denser, and thereby the exponent should decrease with the molecular density, in agreement with microrheological experiments [6,9,36]. Moreover, network statistics also show that the number of effective force-bearing crosslinkers increases with the external strain due to molecular alignment with the stretch direction. As a result of network structure change, the exponent should decrease with the strain, in consistency with previous simulations [20] and experiments on soft glassy colloids [22]. Counterintuitively, however, the strain effect on an exponent cannot be explained by the molecular rotation directly, which was previously conjectured to be able to solidify the network. These results complete a closed loop that explains how the power-law relaxation of the cell cortex is governed by its topological structure, whereby the crosslinker number and imposed strain may decrease the scaling exponent.

ACKNOWLEDGMENTS

This work is supported by the National Natural Science Foundation of China (Grant No. 12072252) and the Fundamental Research Funds for the Central Universities.

APPENDIX A: LENGTH-ENERGY EQUIVALENCE

Here we derive the dissociation rate of a crosslinker bound to a *semiflexible* filament [20]. Consider a representative

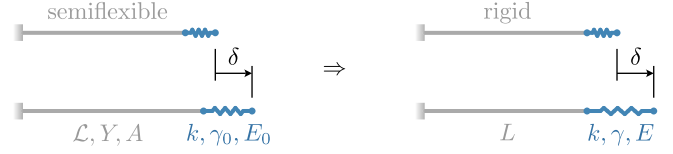


FIG. 6. Representative filament-crosslinker complex. The semiflexible filament is described by the length \mathcal{L} , modulus Y and cross-sectional area A , and the crosslinker is described by the stiffness k , rate constant γ_0 , and binding energy E_0 . With effective rate constant γ and binding energy E , their dissociation dynamics is equivalent to that of a crosslinker bound to a rigid filament of fixed length L .

filament-crosslinker complex (Fig. 6), where the filament is semiflexible, with rest length \mathcal{L} , elastic modulus Y , and cross-sectional area A , whereas the crosslinker is elastic, with stiffness k , rate constant γ_0 , and binding energy E_0 . When the complex is subjected to a deformation δ , the crosslinker extension reads

$$\Delta = \left(\frac{1}{k} + \frac{\mathcal{L}}{YA} \right)^{-1} \frac{\delta}{k} = \left(1 + \frac{k\mathcal{L}}{YA} \right)^{-1} \delta. \quad (\text{A1})$$

Since the stiffness of a crosslinker is much smaller than that of a filament of typical length [40,41], the dissociation rate can be derived in the condition of $k\mathcal{L}/YA \ll 1$ as below:

$$\begin{aligned} \Gamma &= \gamma_0 \exp \left[- \left(E_0 - \frac{k\Delta^2}{2} \right) / \xi \right] \\ &= \gamma_0 \exp \left[- \left(E_0 - \frac{k}{2} \left(1 + \frac{k\mathcal{L}}{YA} \right)^{-2} \delta^2 \right) / \xi \right] \\ &\approx \gamma_0 \exp \left\{ - \left[E_0 - \frac{k}{2} \left(1 - \frac{2k\mathcal{L}}{YA} \right) \delta^2 \right] / \xi \right\} \\ &= \gamma_0 e^{-E_0/\xi} \exp \left[- \left(\frac{k^2\delta^2\mathcal{L}}{YA} - \frac{k\delta^2}{2} \right) / \xi \right]. \end{aligned} \quad (\text{A2})$$

Note that Δ (crosslinker extension in the first line) is eventually replaced by δ (complex deformation in the last line) in the above equation. Hence, the dissociation of a crosslinker bound to a semiflexible filament can be treated as that of a crosslinker bound to a *rigid* filament, with the newly defined rate constant $\gamma = \gamma_0 e^{-E_0/\xi}$ and binding energy $E = k^2\delta^2\mathcal{L}/YA \propto \mathcal{L}$. Since \mathcal{L} is exponentially distributed in the cell cortex [30,31], the binding energy E is also exponentially distributed in Eq. (1) in the main text.

APPENDIX B: UNBINDING STRENGTH

Here we discuss the setting of binding energy η and thermal energy ξ in our model. Their scale is related to the form of strain energy in the dissociation rate, and their values are related to the unbinding strength of a typical crosslinker. In Eq. (1), we construct the strain energy as $kl_0^2\varepsilon^2/2$, which is proportional to the strain squared. With $k = 16$ pN/nm, $l_0 = 50$ nm, and a typical strain of 10%, the scale of strain

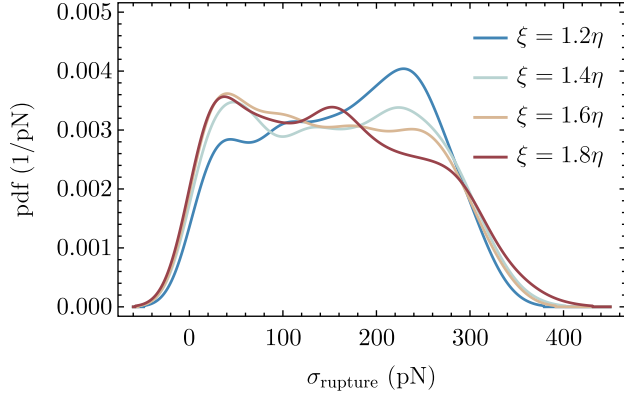


FIG. 7. Unbinding strength distributions of a typical crosslinker under thermal energies $\xi = \{1.2, 1.4, 1.6, 1.8\} \times \eta = 250 k_B T$, under a loading rate of 20 pN/s.

energy may be estimated as

$$U_{\text{scale}} = \frac{16 \text{ pN/nm} \times (5 \text{ nm})^2}{4 \text{ pN nm}} \times 1 k_B T = 100 k_B T. \quad (\text{B1})$$

Accordingly, to match the scale of strain energy, reasonable binding and thermal energies should be several hundreds of $k_B T$ as well, and they can be regarded as effective energies corresponding with such formulation of dissociation rate.

Setting $\xi = 1.2\eta = 250 k_B T$ and $\gamma = 0.15 \text{ s}^{-1}$, we simulate the unbinding force of crosslinkers under a loading rate of 20 pN/s for 10^3 times using Eq. (1), as shown in Fig. 7. The strength distribution is of a bell shape roughly, with a mean value of 162 pN, basically conforming to the experimental measurements on actin-binding-protein filamin [33]. However, when the thermal energy increases to $\xi = 1.8\eta$, the most probable strength is severely reduced, and the distribution becomes a decreasing curve, deviating from the experimental distribution [33]. This is because the binding is largely impaired under very strong thermal agitation. Therefore, we assign $\xi = 1.2\eta$ throughout this study.

APPENDIX C: NETWORK GENERATION

Here we briefly summarize the details on the generation of the network model. Based on the analysis in Appendix A, we treat filaments as rigid rods with fixed length $L = 500 \text{ nm}$, and crosslinkers as linear springs with stiffness $k = 16 \text{ pN/nm}$ and rest length $l_0 = 50 \text{ nm}$.

In the initial configuration, a total number of $N = 500$ filaments are put into a box of side length $W = 1 \mu\text{m}$ and thickness $h = 250 \text{ nm}$, with periodic boundary conditions in x and y directions. The position of a filament is described by a vector \mathbf{P} , and the orientation is described by a vector \mathbf{n} , as shown in Fig. 8(a). Filament position and orientation are uniformly distributed, and set as follows:

$$P_x = u \times W, \quad P_y = u \times W, \quad P_z = u \times W, \quad (\text{C1})$$

$$\theta = \arccos[(1 - 2u) \times \sin(\theta_0/2)], \quad \phi = u \times 2\pi, \quad (\text{C2})$$

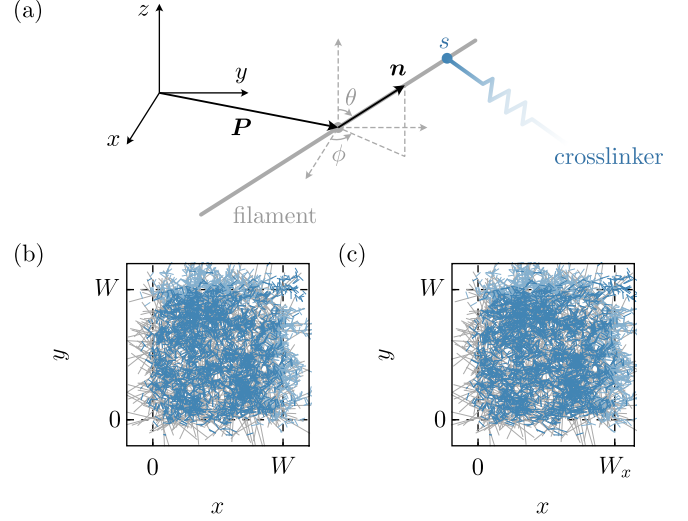


FIG. 8. (a) Description of filament and crosslinker configuration. (b) Top view of the initial configuration of a network with side length W and thickness h , where gray molecules are filaments and blue ones are crosslinkers. (c) Network configuration under a uniaxial strain $\epsilon_x = 5\%$ in the x direction.

where u is a random number uniformly distributed on $[0, 1]$ and regenerated each time, and $\theta_0 = \pi/8$ is an arbitrary angle to restrict out-of-plane inclination. Then, a total number of $n \sim 10^3$ crosslinkers are put onto the filament backbone. Crosslinker configuration is described by the linear coordinates $\{s_i, s_j\}$ of its binding sites on the two bound filaments $\{i, j\}$, as shown in Fig. 8(a). The crosslinker length is then written as

$$l = \|(\mathbf{P}_i + s_i \mathbf{n}_i) - (\mathbf{P}_j + s_j \mathbf{n}_j)\|, \quad (\text{C3})$$

which must be close to the rest length l_0 . Such configuration can be set by searching for binding sites randomly. First, randomly choose two filaments. Second, randomly change the linear coordinates of two potential binding sites on the filaments. Third, check whether their distance is close to l_0 . Repeating the above operations will eventually find suitable binding sites for all crosslinkers. A technical detail here is that, for the convenience of setting initial configurations, the crosslinker end is actually attached with a tiny flexible rope with a length of $l_{\text{end}} = 0.5 \text{ nm}$, such that no force or deformation energy is produced within a tiny range $|l - l_0| < 2l_{\text{end}}$, where the factor 2 comes from the fact that one crosslinker has two ends. Due to the periodic boundary conditions, filaments in adjacent boxes may be connected by crosslinkers [seen as lighter ones in Figs. 8(b) and 8(c)]. Since this work mainly considers typical actin-crosslinking proteins such as filamin, α -actinin, fimbrin, and spectrin, each of which has two actin-binding sites [42], we neglect the multiple binding scenario.

When the network is subjected to a uniaxial strain ϵ_x implemented by changing the side length W_x of the box and the x coordinates of filament centers proportionally, its equilibrium configuration can be obtained through the standard Metropolis algorithm. First, randomly change the position and orientation of a crosslinker. Second, calculate the energy change ΔU .

Third, accept the new configuration if

$$\exp(-\Delta U/k_B T) > u, \quad (\text{C4})$$

where u is a random number uniformly distributed on $[0,1]$ and regenerated each time. Repeating the above operations will eventually lead to a series of thermodynamic equilibrium states of the system.

It is worth mentioning that once the rate is given, time-dependent stochastic dissociation of crosslinkers can be simulated through the Gillespie algorithm as well. In this work, the network model is merely used for the statistics of molecular chain length and crosslinker strain distribution at time $t = 0$. More details can be found in Ref. [20].

APPENDIX D: GRAPH REPRESENTATION OF NETWORK

Here we briefly summarize the concept of graph distance in graph theory, which we use to characterize the topological structure of our networks. As illustrated in Fig. 9, a network can be represented by a graph, with each filament represented by a vertex and each crosslinker by an edge that connects two vertices. In the graph (network), two vertices (filaments) may be connected by a path (molecular chain) formed by a sequence of consecutive vertices and edges. The length of a path (chain) is simply the number of edges (crosslinkers) on it. When several paths are present, their lengths could be different. Graph distance d_{ij} is defined as the minimum length of all paths connecting a vertex pair $\{i, j\}$, and can be generally determined by Dijkstra's algorithm [37]. When averaged over all vertex pairs, $\langle d_{ij} \rangle$ measures the mean length of force-bearing chains in the network, which is abstracted as the chain length d in the minimal model.

APPENDIX E: CATCH-BOND CASE

Here we discuss the case of catch bond. For the catch-bond case, the dissociation rate in Eq. (1) may be modified as

$$\Gamma = \gamma \exp \left[- \left(E + \frac{k l_0^2 \varepsilon^2}{2} \right) / \xi \right], \quad (\text{E1})$$

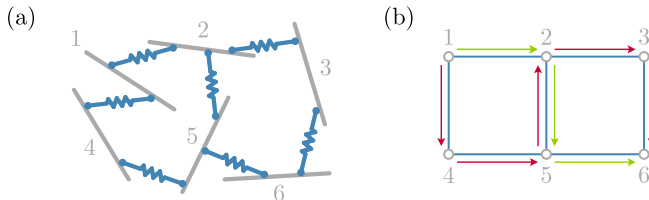


FIG. 9. Graph representation of a network. (a) A local network of six filaments (marked by numbers) and seven crosslinkers. (b) Graph of the network, where vertices and edges represent filaments and crosslinkers, respectively. Vertex 1 and vertex 6 can be connected by several paths, such as the green one $1 \rightarrow 2 \rightarrow 5 \rightarrow 6$ or the red one $1 \rightarrow 4 \rightarrow 5 \rightarrow 2 \rightarrow 3 \rightarrow 6$. Since the length of the former is 3, while the length of the latter is 5, the graph distance between them is $d_{16} = 3$.

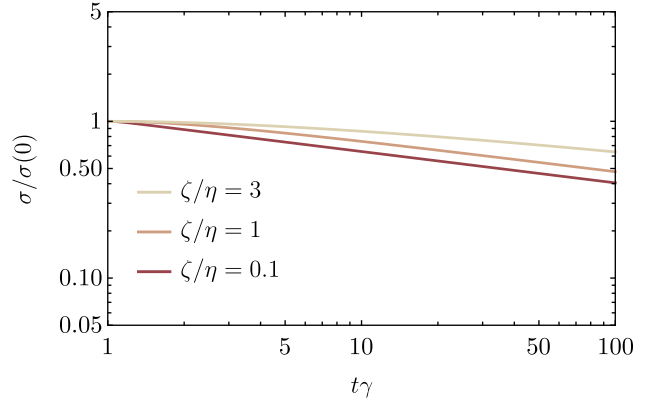


FIG. 10. Relaxation of the minimal model without in-series structure in the catch-bond case.

where the sign of strain energy becomes positive. This changes the form of the minimum mean lifetime of crosslinkers [Eq. (4)] into

$$\tau_m = \gamma^{-1} \exp(k l_0^2 \varepsilon^2 / 2\xi), \quad (\text{E2})$$

which grows with the global strain ε now. Hence, the power-law relaxation will be postponed under large global strains, but neither the power-law feature nor the power-law exponent will be altered, since Eq. (4) does not depend on the specific form of τ_m . Such a modification will not change the form of Eq. (5) either, which does not depend on τ_m explicitly. In addition, as the statements of Secs. III B and III C are based on the *initial* configuration of the network, unrelated to the dissociation dynamics, this modification will not change other green parts of the signaling cascade in Fig. 1(b).

For Sec. III D, the lifetime is now written as

$$\hat{\tau} = \gamma^{-1} e^{(E+\Psi)/\xi}, \quad (\text{E3})$$

where $\hat{\tau} \in (\gamma^{-1}, \infty)$. If we arbitrarily choose the strain energy distribution as $h(\Psi) \propto \exp(-\Psi/\zeta)$ in Eq. (6), we have

$$\begin{aligned} \mathfrak{S}(\hat{\tau}') &= \Pr(\hat{\tau} > \hat{\tau}') \\ &= \iint_{E+\Psi > \xi \ln(\hat{\tau}')} P(E) h(\Psi) dE d\Psi \\ &\propto (\hat{\tau}' \gamma)^{-\beta(1)} - \zeta (\eta^{-1} - \xi^{-1}) (\hat{\tau}' \gamma)^{-\xi/\zeta}, \quad (\text{E4}) \end{aligned}$$

for $\hat{\tau}' > \gamma^{-1}$. We plot the stress history $\sigma(t)/\sigma(0) = \mathfrak{S}(t)$ under different values of ζ/η in Fig. 10. It can be seen that the exponent slightly decreases as the strain energy variance ζ increases (corresponding to the smaller global strain exerted on the network). This suggests that the exponent increase under small global strain may still be induced by the topological mechanism in the case of catch bond.

- [1] P. Kollmannsberger and B. Fabry, *Annu. Rev. Mater. Res.* **41**, 75 (2011).
- [2] X. Trepas, G. Lenormand, and J. J. Fredberg, *Soft Matter* **4**, 1750 (2008).
- [3] P. Kollmannsberger, C. T. Mierke, and B. Fabry, *Soft Matter* **7**, 3127 (2011).
- [4] M. Bolland, N. Desprat, D. Icard, S. Fereol, A. Asnacios, J. Browaeys, S. Henon, and F. Gallet, *Phys. Rev. E* **74**, 021911 (2006).
- [5] N. Desprat, A. Richert, J. Simeon, and A. Asnacios, *Biophys. J.* **88**, 2224 (2005).
- [6] N. Bonakdar, R. Gerum, M. Kuhn, M. Sporrer, A. Lippert, W. Schneider, K. E. Aifantis, and B. Fabry, *Nat. Mater.* **15**, 1090 (2016).
- [7] N. Khalilgharibi, J. Fouchard, N. Asadipour, R. Barrientos, M. Duda, A. Bonfanti, A. Yonis, A. Harris, P. Mosaffa, Y. Fujita *et al.*, *Nat. Phys.* **15**, 839 (2019).
- [8] J. S. de Sousa, R. S. Freire, F. D. Sousa, M. Radmacher, A. F. B. Silva, M. V. Ramos, A. C. O. Monteiro-Moreira, F. P. Mesquita, M. E. A. Moraes, R. C. Montenegro *et al.*, *Sci. Rep.* **10**, 4749 (2020).
- [9] J. Hu, Y. Li, Y. Hao, T. Zheng, S. K. Gupta, G. A. Parada, H. Wu, S. Lin, S. Wang, X. Zhao *et al.*, *Proc. Natl. Acad. Sci. USA* **116**, 17175 (2019).
- [10] E. Moeendarbary, L. Valon, M. Fritzsche, A. R. Harris, D. A. Moulding, A. J. Thrasher, E. Stride, L. Mahadevan, and G. T. Charras, *Nat. Mater.* **12**, 253 (2013).
- [11] B. Fabry, G. N. Maksym, J. P. Butler, M. Glogauer, D. Navajas, and J. J. Fredberg, *Phys. Rev. Lett.* **87**, 148102 (2001).
- [12] B. D. Hoffman, G. Massiera, K. M. Van Citters, and J. C. Crocker, *Proc. Natl. Acad. Sci. USA* **103**, 10259 (2006).
- [13] D. Stamenovic, B. Suki, B. Fabry, N. Wang, and J. J. Fredberg, *J. Appl. Physiol.* **96**, 1600 (2004).
- [14] B. Fabry, G. N. Maksym, J. P. Butler, M. Glogauer, D. Navajas, N. A. Taback, E. J. Millet, and J. J. Fredberg, *Phys. Rev. E* **68**, 041914 (2003).
- [15] J. Xu, D. Wirtz, and T. D. Pollard, *J. Biol. Chem.* **273**, 9570 (1998).
- [16] J. Plagge, A. Fischer, and C. Heussinger, *Phys. Rev. E* **93**, 062502 (2016).
- [17] G. H. Koenderink, Z. Dogic, F. Nakamura, P. M. Bendix, F. C. MacKintosh, J. H. Hartwig, T. P. Stossel, and D. A. Weitz, *Proc. Natl. Acad. Sci. USA* **106**, 15192 (2009).
- [18] Y. Mulla, F. C. MacKintosh, and G. H. Koenderink, *Phys. Rev. Lett.* **122**, 218102 (2019).
- [19] M. L. Gardel, F. Nakamura, J. Hartwig, J. C. Crocker, T. P. Stossel, and D. A. Weitz, *Phys. Rev. Lett.* **96**, 088102 (2006).
- [20] S. H. Li, H. Gao, and G. K. Xu, *Biophys. J.* **121**, 4091 (2022).
- [21] T. Kim, W. Hwang, and R. D. Kamm, *Biophys. J.* **101**, 1597 (2011).
- [22] P. Agarwal and L. A. Archer, *Phys. Rev. E* **83**, 041402 (2011).
- [23] S. L. Freedman, G. M. Hocky, S. Banerjee, and A. R. Dinner, *Soft Matter* **14**, 7740 (2018).
- [24] S. Fielding, Ageing, driving and effective temperatures from “soft rheology” to glassy dynamics, Doctoral dissertation, University of Edinburgh, United Kingdom, 2000.
- [25] P. Sollich, *Phys. Rev. E* **58**, 738 (1998).
- [26] P. Sollich, F. Lequeux, P. Hébraud, and M. E. Cates, *Phys. Rev. Lett.* **78**, 2020 (1997).
- [27] J. T. Hang, G. K. Xu, and H. Gao, *Sci Adv* **8**, eabn6093 (2022).
- [28] J. T. Hang, Y. Kang, G. K. Xu, and H. Gao, *Nat. Commun.* **12**, 6067 (2021).
- [29] G. I. Bell, *Science* **200**, 618 (1978).
- [30] M. Fritzsche, C. Erlenkamper, E. Moeendarbary, G. Charras, and K. Kruse, *Sci. Adv.* **2**, e1501337 (2016).
- [31] S. Burlacu, P. A. Janmey, and J. Borejdo, *Am. J. Physiol.* **262**, C569 (1992).
- [32] P. Chugh *et al.*, *Nat. Cell. Biol.* **19**, 689 (2017).
- [33] J. M. Ferrer, H. Lee, J. Chen, B. Pelz, F. Nakamura, R. D. Kamm, and M. J. Lang, *Proc. Natl. Acad. Sci. USA* **105**, 9221 (2008).
- [34] D. T. Gillespie, *J. Comput. Phys.* **22**, 403 (1976).
- [35] R. Erban, J. Chapman, and P. Maini, *arXiv:0704.1908*.
- [36] G. Lenormand, E. Millet, B. Fabry, J. P. Butler, and J. J. Fredberg, *J. R. Soc. Interface* **1**, 91 (2004).
- [37] D. B. West, *Introduction to Graph Theory* (Prentice Hall, Upper Saddle River, 2001), Vol. 2.
- [38] D. Frenkel and B. Smit, *Understanding Molecular Simulation: From Algorithms to Applications* (Elsevier, New York, 2001), Vol. 1.
- [39] R. Phillips, J. Kondev, J. Theriot, and H. Garcia, *Physical Biology of the Cell* (Garland Science, New York, 2012).
- [40] C. P. Broedersz, C. Storm, and F. C. MacKintosh, *Phys. Rev. E* **79**, 061914 (2009).
- [41] A. Shamloo and B. Mehrafrooz, *Cytoskeleton (Hoboken)* **75**, 118 (2018).
- [42] B. Alberts, A. Johnson, J. Lewis, D. Morgan, M. Raff, K. Roberts, P. Walter, J. Wilson, and T. Hunt, *Molecular Biology of the Cell* (W. W. Norton & Company, New York, 2017).